I&EC research
Industrial & Engineering Chemistry Research

Article

pubs.acs.org/IECR

Stochastic Optimal Control of Seeded Batch Crystallizer Applying the Ito Process

Kirti M. Yenkie and Urmila Diwekar*

Department of Bioengineering, University of Illinois, Chicago, Illinois 60607, United States

Center for Uncertain Systems: Tools for Optimization & Management (CUSTOM), Vishwamitra Research Institute, Clarendon Hills, Illinois 60514, United States

ABSTRACT: Minimization of operation costs and the enhancement in product quality have been major concerns for all industrial processes. Predetermined operating conditions can help to achieve the goals for efficient production. These conditions can be determined using an optimal control analysis of batch crystallization process characterized by determination of the time-varying profiles for process parameters. Batch crystallization is associated with parameters such as temperature, supersaturation, and agitation. Some process parameters, such as solubility and crystal lattice, are functions of fundamental properties of the system. Thus, the process parameters can have various associated physical and engineering sources of uncertainties, which, in turn, would prevent the real process operation to be optimal. These static uncertainties result in dynamic uncertainties, because of the unsteady state nature of the process. This paper presents a novel approach to solve optimal control problems in batch crystallization involving uncertainties. These uncertainties are modeled as a special class of stochastic processes called Ito processes. The resulting stochastic optimal control problem is solved using Ito's Lemma, stochastic calculus, and stochastic maximum principle. The comparison between the results for the deterministic and the stochastic optimal temperature profile show that, when uncertainties are present, the stochastic optimal control approach presented in this paper gives better results, in terms of maximum crystal growth, represented in terms of crystallization moments. Percentage improvements of ∼3% and ∼6% are observed for the stochastic optimal profile, in comparison to the deterministic and linear cooling cases, in the presence of parametric uncertainty.

1. INTRODUCTION

Batch crystallization is widely used in chemical, pharmaceutical, photographic, and other manufacturing processes for the preparation of crystalline products with several desirable attributes. The equipment is relatively simple and manageable in processes that involve toxic and highly poisonous substances. These are more economical, requiring minimum development and modification time, compared to their continuous counterparts. Batch crystallization is very useful in industries with frequently changing recipes and product lines, as reported by Costa et al.[1] Also, the batch system helps to obtain a narrower particle size distribution (PSD) with high crystal purity. The crystallization process has an influence on the downstream processing and, hence, reproducible PSD in each operation is of prime importance. Thus, it is essential to find the variables affecting the process and control them within an acceptable range, to satisfy the final product quality requirements. The challenge is to operate the batch crystallizer under specific conditions, to obtain crystals with the desired attributes.

Some fundamental aspects (Hill et al.[2]) of crystallization will be discussed to understand the batch crystallization system in a better way. The basic phenomena influencing crystallization include solid−liquid equilibria; the material will not crystallize unless the solution is supersaturated. Supersaturation[2] is a condition in which the solute concentration in the solution is higher than the solubility. It is the driving force for the crystallization process and is expressed in terms of concentration. It can be expressed as a difference (ΔC) in the concentration of the solute and its saturation concentration or as a supersaturation ratio (S); it is also known as the relative supersaturation.

$$\text{Supersaturation} = \Delta C = C - C_s \tag{1}$$

$$\text{Relative supersaturation} = S = \frac{\Delta C}{C_s} \tag{2}$$

The above thermodynamic information gives an idea about the maximum amount of material that will crystallize as a solid; however, to gain insight into the rate of the production of crystals, we need information about its kinetics. The crystallization kinetics provides design information such as crystal production rate, size distribution, and its shape. The kinetics is divided into four mechanisms: growth, nucleation, agglomeration, and breakage. Growth refers to the increase in crystal size due to addition of solute molecules to the existing crystals. Nucleation refers to the formation of new solid particles from the solution or formation of small clusters by solute molecules. Agglomeration occur when two particles collide and stick together to form a larger particle. Breakage occurs in stirred vessels; the larger particle breaks into smaller fragments, because of attrition. The phenomena of agglomeration and breakage are rare

Special Issue: L. T. Fan Festschrift

Received: February 23, 2012
Revised: April 30, 2012
Accepted: May 16, 2012
Published: May 16, 2012

   dx.doi.org/10.1021/ie300491v | Ind. Eng. Chem. Res. 2013, 52, 108−122

events and are often neglected while modeling the crystallization process.

The literature on crystallization kinetics[2−4] have discussed several mathematical expressions, depending upon the process complexity for each of the mentioned mechanisms. For example, growth can be size-independent or size-dependent; it can have a constant value or it may be a function of a thermodynamic parameter such as solubility. Thus, the selection of proper kinetics specific to the batch crystallization process is an essential part of process modeling.

The evolution of supersaturation in time affects almost all the kinetic phenomena occurring in the crystallization process. In cooling crystallization, supersaturation magnitude is determined by the cooling rate, and, hence, optimization of cooling trajectory has been the main focus of the research activity. Many researchers have contributed to problems for the purpose of finding the best operating policies in batch crystallization processes. In general, two classes of operating policies have been proposed in the literature by Ward et al.,[5] and their choice is dependent upon the process application. It may be an early growth policy, where the formation of nuclei is minimized, since supersaturation is the greatest at the start of the process or a late growth policy, where the formation of nuclei is preferred, since supersaturation is greatest toward the end of the process.

Determination of the optimal temperature or supersaturation trajectory for a seeded batch crystallizer is the most well-studied problem in chemical engineering, apart from batch reactors and batch distillation. The concept of programmed cooling in batch crystallizers was first discussed by Mullin and Nyvlt in 1971.[6] They studied the laboratory-scale crystallization of potassium sulfate and ammonium sulfate using a temperature controller and observed improvement in the crystal size and quality under programmed cooling. Later, in 1974, A. G. Jones[7] presented a mathematical theory based on moment transformations of population balance equations. He used the continuous maximum principle to predict optimal cooling curves. Rawlings et al.[8] discussed issues in crystal size measurement using laser light scattering experiments and optimal control problem formulation. In 1994, Miller and Rawlings[9] discussed the uncertain bounds on model parameter estimates for a batch crystallization system. The cooling profile sensitivity was analyzed by small perturbations in the model parameters. Optimal temperature prediction for batch crystallization has also been done by Hu et al.,[10] Shi et al.,[11] Paengjuntuek et al.,[12] and Corriou and Rohani.[13]

Previous literature on particulate processes have mentioned several sources of model uncertainties, such as partially known time-varying process parameters, exogenous disturbances, and unmodeled dynamics of the controller, used as discussed by Chiu and Christofides.[14] They modeled the population balances with time-varying uncertainties like pre-exponential factor in nucleation rate and crystal density for a continuous crystallizer with fines trap for robust controller design based on Lyapunov's method, using the method of finite-dimensional approximations and the method of weighted residuals.

Stochastic modeling of particulate processes and parameter estimation using the experimentally measured particle sizes has also attracted many researchers. Grosso et al.[15] presented a stochastic approach for modeling PSD and comparative assessments of different models. The experimental data were modeled using the Langevin equations with different values of the diffusion coefficient. Incorporation of this in the PBE model resulted in the development of the Fokker−Planck equation, which was used for the simulated value prediction of the evolution of crystal size in the kinetic inversion problem. Dynamic modeling was done by Laloue et al.[16] to incorporate the agglomeration and breakage effects in the population balances. The model was validated using experimental crystal size distribution (CSD) measurements.

Ma et al.[17] presented a worse-case performance analysis of optimal control trajectories by considering features such as the computational effort, parametric uncertainty and control implementation inaccuracies. The objectives were the deviations in the optimal trajectory predicted by the model and the optimal trajectory for the real system, in terms of weighted Euclidean norms. They predicted the worse-case parameter vector and the worse-case control move, thus predicting the maximum positive or negative deviation in each of the model parameters. They applied the strategy to crystallization process in which they selected several objectives, depending on product quality. The results helped to decide whether more experiments are needed to produce parameter estimates of higher accuracy. They predicted that the ratio of nucleated crystal mass to seeded crystal mass was most sensitive to parametric uncertainty. In 2001, Ma and Braatz[18] extended the same methodology to performance objectives in crystal shape prediction for applications to multidimensional crystallization processes. Thus, we use parametric uncertainty as a major criterion for stochastic optimal control.

The focus of the current work is to propose a new approach to handle parametric uncertainties in mathematical formulations of batch crystallization process. A case study for the seeded batch crystallization is presented to demonstrate the methodology. The novelty lies in the method of characterizing the uncertainty and then propagating it in the model to study its effect on the optimal control and overall process performance. The static kinetic parameter uncertainty is modeled using a Gaussian distribution. This static uncertainty results in dynamic uncertainty within the process, which can be modeled as an Ito process.[19] The application of Ito processes to batch crystallization modeling and the stochastic optimal control policy results in better performance than the deterministic methods, because the process uncertainties are represented within the model.

2. MODELING A SEEDED BATCH CRYSTALLIZER

Particulate processes are characterized by properties such as particle shape, size, surface area, mass, and product purity. In crystallization, the particle size and total number of crystals vary with time. A population balance formulation describes the process of crystal size distribution with time most effectively. Thus, modeling of a batch crystallizer involves the use of population balances to model the crystal size prediction and the mass balance on the system can be modeled as a simple differential equation having concentration as the state variable. The population balance can be expressed as eq 3:[10,11]

$$\frac{\partial n(r,t)}{\partial t} + \frac{\partial (G(r,t)n(r,t))}{\partial r} = B \tag{3}$$

where n is the number density distribution, t is the time, r represents the characteristic dimension for size measurements, G is the crystal growth rate, and B is the nucleation rate. Both growth and nucleation processes describe crystallization kinetics, and their expression may vary, depending on the system under consideration. In this work, the system under consideration is potassium sulfate, which has been studied earlier by Hu et al.,[10] Shi et al.,[11] and Paengjuntuek et al.[12]

dx.doi.org/10.1021/ie300491v | Ind. Eng. Chem. Res. 2013, 52, 108−122

From the previous work, the following kinetic expressions have been most appropriate in representing the behavior of the system:

(a) Nucleation kinetics:[10−12]

$$B(t) = k_b \exp\left(\frac{-E_b}{RT}\right)\left(\frac{C - C_s(T)}{C_s(T)}\right)^b \mu_3(t) \tag{4}$$

(b) Growth kinetics:[10−12]

$$G(t) = k_g \exp\left(\frac{-E_g}{RT}\right)\left(\frac{C - C_s(T)}{C_s(T)}\right)^g \tag{5}$$

where k_b and k_g are constants of the system, E_b and E_g are activation energies, and b and g are exponents of nucleation and growth, respectively. $C_s(T)$ is the saturation concentration at a given temperature. The following equations are used to evaluate the saturation and metastable concentrations corresponding to the solution temperature T (expressed in units of °C).[11]

$$C_s(T) = 6.29 \times 10^{-2} + 2.46 \times 10^{-3}T - 7.14 \times 10^{-6}T^2 \tag{6}$$

$$C_m(T) = 7.76 \times 10^{-2} + 2.46 \times 10^{-3}T - 8.10 \times 10^{-6}T^2 \tag{7}$$

The mass balance, in terms of concentration of the solute in the solution, is expressed as the differential equation shown as eq 8:

$$\frac{dC}{dt} = -3\rho k_v G(t)\mu_2(t) \tag{8}$$

where ρ is the density of the crystals, k_v the volumetric shape factor, and μ_2 is the second moment of particle size distribution (PSD).

Since $n(r,t)$ represents the population density of the crystals,[3] the ith moment of the particle size distribution (PSD) is given by eq 9:

$$\mu_i = \int_0^\infty r^i n(r, t)\, dr \tag{9}$$

Each moment signifies a characteristic of the crystal.[3] Thus, depending upon the desired characteristics, optimization objectives are simpler to formulate, in terms of crystallization moments. The zeroth moment corresponds to the particle number, the first moment corresponds to the particle size or shape, the second moment corresponds to its surface area, and the third moment corresponds to the particle volume.

Since population balance equations are multidimensional, their implementation in control functions is tedious; hence, much research has been focused on the model order reduction methods. One of the most common and efficient reduction methods is the method of moments. There are other methods for solving PBEs, such as the discretization methods,[20] method of characteristics, successive approximation,[21] etc. For simplifying the solution method, we reduce the population balance equations into moment balance equations. It is also advantageous, since it is difficult and time-consuming to formulate an optimization problem involving PBEs. Thus, the moment model leads to a reduced-order model involving the process dynamics in batch crystallization.

The moment model approach provides a set of ordinary differential equations (ODEs). From the definition of the ith moment in eq 9, we can convert the population balance in eq 3 to moment equations by multiplying both sides by r^i, and integrating over all particle sizes. Fourth-order moments and higher do not affect third-order moments and lower, implying that only the first four moments and concentration can adequately represent the crystallization dynamics.[11] Separate moment equations are used for the seed and nuclei classes of crystals, and they are defined as

$$\mu_i^{\,n} = \int_0^{r_g} r^i n(r, t)\, dr \tag{10}$$

$$\mu_i^{\,s} = \int_{r_g}^\infty r^i n(r, t)\, dr \tag{11}$$

where the superscript "n" represents nucleation and the superscript "s" represents seed, r_g is the critical radius that distinguishes the two groups. Since, we ignore the agglomeration and breakage phenomena, the number of seeds added to the process (μ_0^s) remain constant. This facilitates, in writing, the desired objective function.

(1) Moment equations for the nucleated crystals:[11,13]

$$\frac{d\mu_0^{\,n}}{dt} = B(t)$$

$$\frac{d\mu_i^{\,n}}{dt} = iG(t)\mu_{i-1}^{\,n}(t) \qquad i = 1, 2, 3 \tag{12}$$

(2) Moment equations for seeded crystals:[11,13]

$$\mu_0^{\,s} = \text{constant}$$

$$\frac{d\mu_i^{\,s}}{dt} = iG(t)\mu_{i-1}^{\,s}(t) \qquad i = 1, 2, 3 \tag{13}$$

The overall ith moments are defined as the summation of nucleated and seeded crystallization moments:

$$\mu_i^{\,t} = \mu_i^{\,n} + \mu_i^{\,s} \tag{14}$$

Values of the kinetic parameters involved in growth and nucleation for potassium sulfate in an aqueous solution are presented in Table 1, taken from previous literature sources.[10−12]

Table 1. Parameter Values for Seeded Batch Cooling Crystallizer[10−12]

parameter	value from experiments/model fitting
	G Kinetics
k_g	1.44×10^8 μm s^{-1}
E_g/R	4859 K
g	1.5
	B Kinetics
k_b	285 (s μm^3)$^{-1}$
E_b/R	7517 K
b	1.45

3. OPTIMAL CONTROL PROBLEMS

Optimal control is useful for deriving information about efficient process design and operation in industries. Optimal control involves the evaluation of time-dependent operating profiles, in terms of the control variable to optimize the process performance. In crystallization, the control variable happens to be the temperature, while the process performance is determined by the crystal size distribution and product yield at

dx.doi.org/10.1021/ie300491v | Ind. Eng. Chem. Res. 2013, 52, 108−122

the final time. These problems can be solved by different methods that are available, such as calculus of variations, dynamic programming, and maximum principle discussed by Diwekar.[19] These methods require proper mathematical representation of the problem and follow a well-defined solution strategy. The prior mentioned methods of calculus of variation and dynamic programming involve second-order differential equations or partial differential equations, respectively, while the maximum principle involves only first-order ODEs. This makes the method more attractive, compared to the other two methods, and hence is employed in this research. Another advantage of using maximum principle lies in the availability of stochastic calculus for solving equations involving uncertainties in their process variables, which shall be explained in detail later in section 5.1.

3.1. Deterministic Optimal Control. For uniformity of shape and size in the crystals in a seeded batch crystallization process, it is essential to ensure that the nucleation phenomena occurs to the minimum and mostly the seeded crystals grow to the desired size at a certain rate. If nucleation occurs in the initial phase, then there is a possibility that the nucleated crystal will compete with the seeded ones; thus, if the phenomena is of late growth, then nucleation in the earlier phase is preferred. Thus, depending on the process operation, many types of objective functions have been proposed.[5] All aim at finding an optimal temperature trajectory during process operation that shall enable the desired crystal size at final time.

Since, the third moment is a representative of volume in crystallization model, it is used in the objective function by most researchers working in the area. We also use the same concept to write the objective function as shown in eq 15:

$$\max_{T(t)}\{\mu_3^{s}(t_f) - \mu_3^{n}(t_f)\} \tag{15}$$

subject to the seeded batch crystallization model, eqs 8, 12, and 13, initial conditions (see Table 2), and the constraints for supersaturation condition maintenance. The aim is to find an optimal temperature trajectory, which minimizes the total volume of fine crystals, represented by the third moment of nucleated crystals (μ_3^{n}) and maximizes the size of seeded crystals represented by the third moment of seeded crystals (μ_3^{s}) in order to satisfy the product quality requirements. Thus, it involves forcing growth by suppressing the nucleation phenomenon.

Table 2. Initial Values of the States of the Model[a]

state	value	state	value
$y_1 = C$	0.1743 g solute/g solvent		
$y_2 = \mu_0^{s}$	66.66	$y_6 = \mu_0^{n}$	0.867
$y_3 = \mu_1^{s}$	1.83×10^4	$y_7 = \mu_1^{n}$	0
$y_4 = \mu_2^{s}$	5.05×10^6	$y_8 = \mu_2^{n}$	0
$y_5 = \mu_3^{s}$	1.93×10^9	$y_9 = \mu_3^{n}$	0
input T (temp)	323 K		

[a]Data taken from refs 10−12.

The active constraint for the concentration condition is listed in eq 16, which is to be maintained at all times.

$$C_s \le C \le C_m \tag{16}$$

Thus, the complete model involving the moment equations will consist of nine state equations (see Appendix A.1). We denote the state variables as y_i for simplicity and better understanding of the maximum principle formulation. The objective function, in terms of y, is given as eq 17 and the state equations in eq 18. The method will involve introduction of nine additional variables, known as adjoints (z_i), corresponding to each of the state variable (y_i), which must satisfy eq 19 and a Hamiltonian, which satisfies the relation described by eq 20.

$$y_i = [C \;\; \mu_0^{s} \;\; \mu_1^{s} \;\; \mu_2^{s} \;\; \mu_3^{s} \;\; \mu_0^{n} \;\; \mu_1^{n} \;\; \mu_2^{n} \;\; \mu_3^{n}]$$

$$\mathrm{Max}_{T(t)}\{y_5(t_f) - y_9(t_f)\} \tag{17}$$

$$\frac{dy_i}{dt} = f(y_i, t, T) \tag{18}$$

$$\frac{dz_i}{dt} = \sum_{j=1}^{9} z_j \frac{\partial f(y_i, t, T)}{\partial y_i} = f(y_i, z_i, t, T) \tag{19}$$

$$H = \sum_{i=1}^{9} z_i f(y_i, t, T) \tag{20}$$

3.2. Solution Methodology. The system results in a two-point boundary value problem, since we have initial conditions for the state variables and final conditions for the adjoint variables.

$$\text{batch time} = 1800 \text{ s } (30 \text{ min})$$

$$y_i(t_0) = [0.1743 \;\; 66.66 \;\; 1.83 \times 10^4 \;\; 5.05 \times 10^6 \;\; 1.93 \times 10^9 \;\; 0.867 \;\; 0 \;\; 0 \;\; 0]$$

$$z_i(t_f) = [0 \;\; 0 \;\; 0 \;\; 0 \;\; 1 \;\; 0 \;\; 0 \;\; 0 \;\; -1]$$

For evaluation of the Hamiltonian derivative, we use an analytical method proposed by Benavides and Diwekar,[22] in which we introduce an additional variable corresponding to each of the state and adjoint variable (see Appendix A.2). The variable θ_i corresponds to each of the state variable y_i and the variable $\oint_i$ corresponds to each of the adjoint variable z_i, respectively.

$$\theta_i = \frac{dy_i}{dT} \quad \text{and} \quad \oint_i = \frac{dz_i}{dT} \tag{21}$$

$$\frac{d\left(\frac{dy_i}{dt}\right)}{dT} = \frac{d\left(\frac{dy_i}{dT}\right)}{dt} = \frac{d\theta_i}{dt} \tag{22}$$

$$\frac{d\left(\frac{dz_i}{dt}\right)}{dT} = \frac{d\left(\frac{dz_i}{dT}\right)}{dt} = \frac{d\oint_i}{dt} \tag{23}$$

$$\frac{dH}{dT} = \sum_{i=1}^{9}\left(\frac{dH}{dy_i}\right)\left(\frac{dy_i}{dT}\right) + \sum_{i=1}^{9}\left(\frac{dH}{dz_i}\right)\left(\frac{dz_i}{dT}\right) \tag{24}$$

The optimal control variable $T(t)$ can be obtained by finding the extremum of the Hamiltonian at each time step, using the optimality condition of $\lceil |dH/dT| \rceil < tolerance$. Since the process has active constraint for maintenance of supersaturation conditions, after computing the temperature, we evaluate the concentration at that time step and compare it first with the saturation concentration (C_s): if the concentration is below this limiting value, we evaluate the temperature using the expression for C_s and proceed to check for the other limiting condition of

dx.doi.org/10.1021/ie300491v | Ind. Eng. Chem. Res. 2013, 52, 108−122

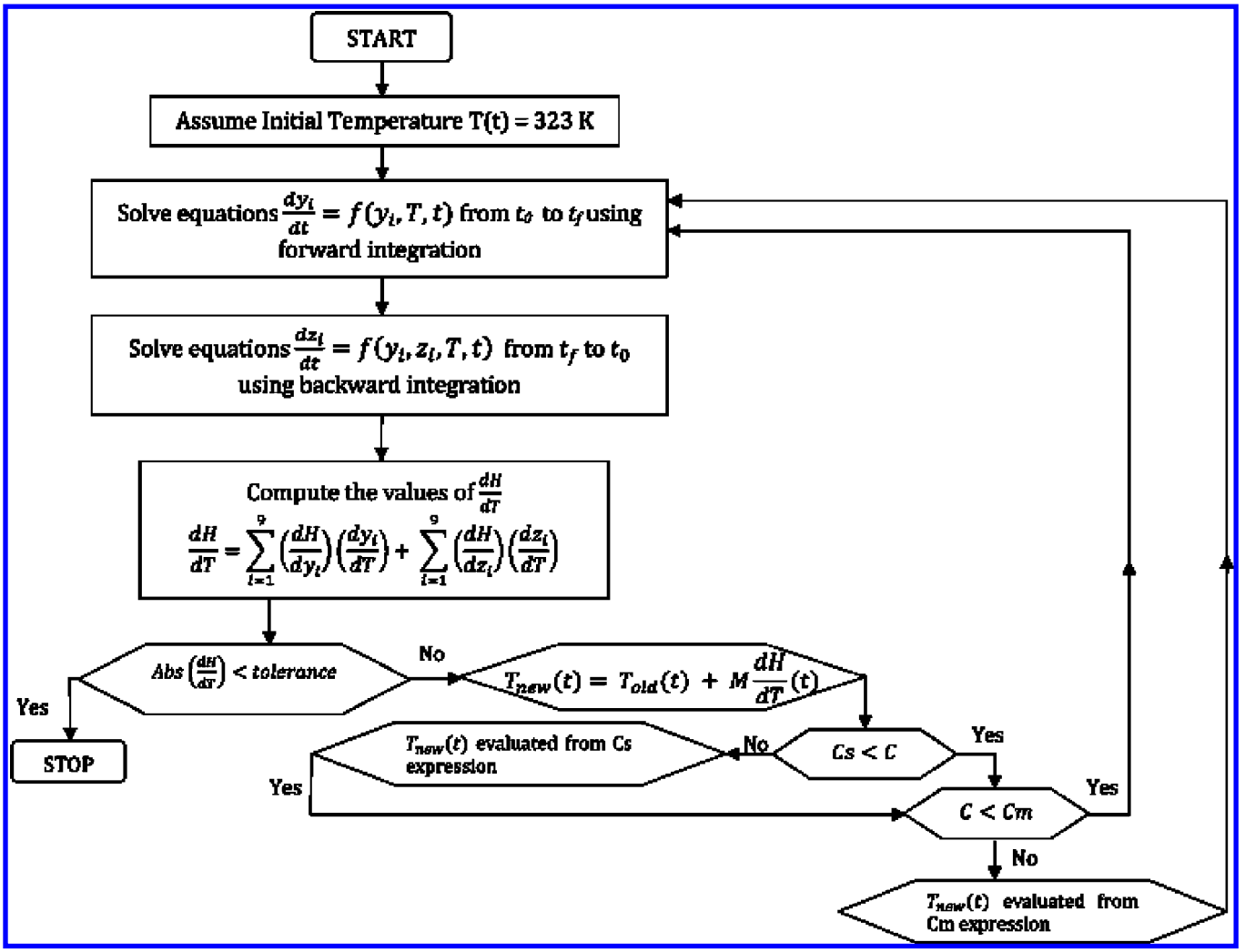

Figure 1. Flowchart for optimal temperature profile evaluation using the maximum principle (active constraint strategy).

the metastable limit concentration (C_m); if concentration evaluated with the temperature is greater than the metastable limit value, we evaluate temperature from the expression for C_m (see Appendix A.3). The flowchart for the process is shown in Figure 1.

3.3. Results. The derivative of Hamiltonian profiles at different iterations is shown in Figure 2. It can be seen that the $|dH/dT|$ value decreases with every iteration. The temperature profiles can be observed in Figure 3 for all iterations and the final iteration is shown as a bold line. At the final iteration, the $|dH/dT|$ value lies within the given tolerance range; hence, we conclude the temperature to be optimum. Figure 4 shows the variation of objective function with time. It can be seen that the optimal value is reached after ~900 s and then the function value remains constant until the total batch time lapses.

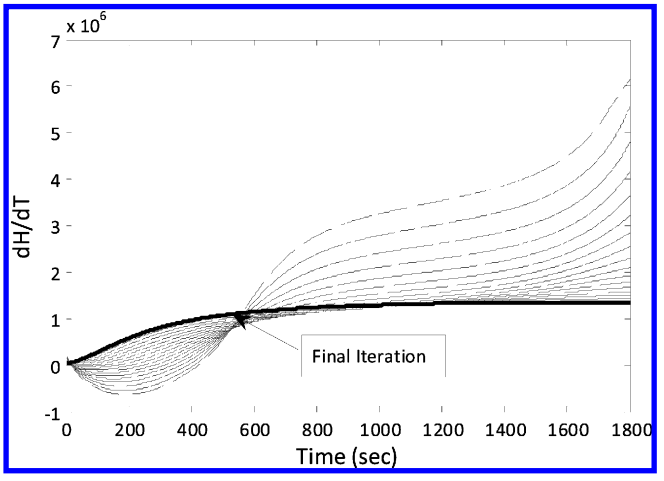

Figure 2. Profiles of Hamiltonian gradients (dH/dT) for all iterations.

4. UNCERTAINTY MODELING AND OPTIMIZATION IN CRYSTALLIZATION

4.1. Uncertainties in Batch Crystallization. The kinetic parameters are generally empirical constants determined by fitting experimental data to the model, and, hence, are a source of uncertainty within the system. In batch crystallization kinetics, the growth and nucleation expressions have empirical constants shown in Table 3, they can be assumed to follow a Gaussian distribution, with the fitted values from previous experiments to be the mean. We assume that the values deviate approximately ±5% about the mean.

We consider a 95% confidence interval and hence, the kinetic parameters lie within two standard deviations of their values ($\mu \pm 2\sigma$). Thus, we evaluate the standard deviation for all of them using the extreme deviations as minimum and maximum values.

dx.doi.org/10.1021/ie300491v | Ind. Eng. Chem. Res. 2013, 52, 108−122

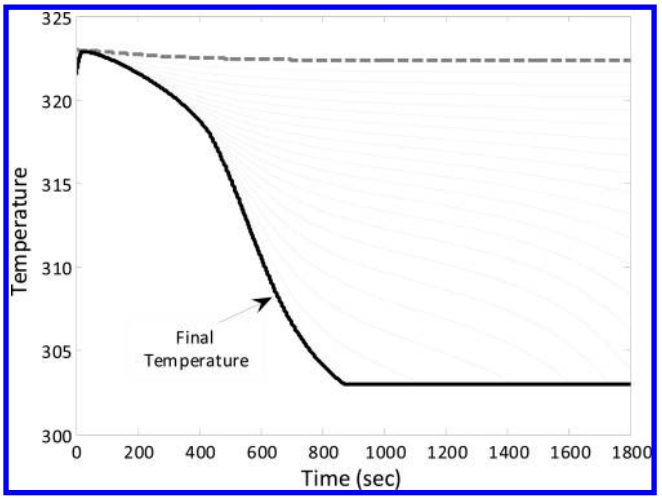

Figure 3. Profiles of temperature for all iterations.

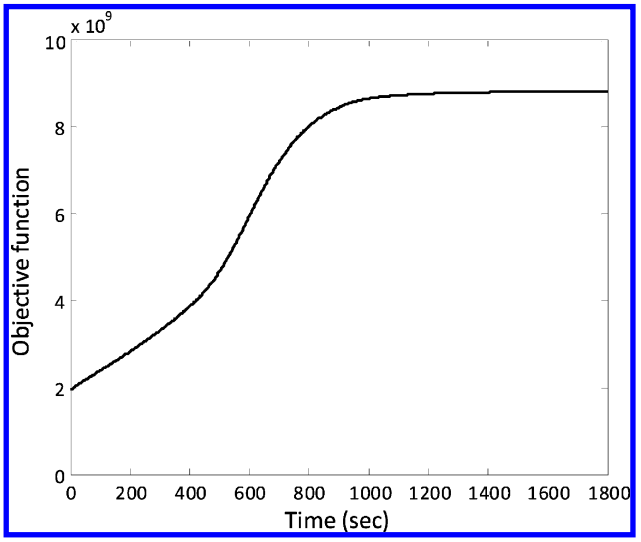

Figure 4. Objective function value $[\mu_3^s(t_f) - \mu_3^n(t_f)]$.

Table 3. Kinetic Parameter Uncertainty in Batch Crystallization Model[a]

kinetic constants	value from experiments/ model fitting	range of values
	Uncertainty G	
k_g	1.44×10^8 μm s^{-1}	1.368×10^8–1.512×10^8
E_g/R	4859 K	4616.05–5101.95
g	1.5	1.425–1.575
	Uncertainty B	
k_b	285 (s $\mu m^3)^{-1}$	270.75–299.25
E_b/R	7517 K	7141.15–7892.85
b	1.45	1.3775–1.5225

[a]Data taken from refs 10–12.

- The sampling operation for multivariable uncertain parameter domain is performed using the Monte Carlo sampling technique, which is based on a pseudo-random generator where samples are drawn from a uniform distribution from 0 to 1 and then inverted using the normal distributions of each parameter.
- 100 sample values for each of the kinetic parameter are generated using inverse transformation over cumulative probability distribution.
- After generating 100 samples for the kinetic parameter data, the model is simulated using each set.
- The resulting dynamic uncertainty in the state variables due to static uncertainty in the kinetic parameters is observed in the plots of the dynamic uncertainty as shown in Figure 5a and 5b.

4.2. Capturing Uncertainties with Ito Processes. From the previous work done by our research group,[19,23−26] it has been shown that the dynamic uncertainties in several processes, such as the batch reactors[24] and batch distillation,[19,25] can be represented using stochastic processes called as the Ito process.[27] These Ito processes were mostly applied in financial field and stock price modeling to model time-dependent uncertainties. We characterize the time-dependent uncertainties in the state variables using Ito processes. The advantage lies in the ability to integrate these equations using the principles of stochastic calculus and use of stochastic maximum principle to solve for optimal temperature profile.

The simplest example of a stochastic process is the Brownian motion, which is also known as the Wiener process in the continuous form. The following three properties are used to characterize an important process as Wiener:[19,24,25,27]

(i) It should follow the Markov property; the probability distribution for all future values of the process is dependent only on its current value.
(ii) It should have independent increments in time
(iii) Changes in the process over a time interval should be normally distributed.

The Ito processes are of various types whose basis is taken from the Wiener processes. Depending on the behavior of the system uncertainty, it can be modeled as a suitable type of Ito process. Examples of Ito processes include simple Brownian motion,[19] geometric Brownian motion,[19] mean reverting process,[19] geometric mean reverting process,[19] etc. Following a similar approach, we aim to model the uncertainties in batch crystallization with Ito processes in order to solve the stochastic optimal control problem, which will provide more insight into the actual process operation.

4.3. Modeling Uncertainties in the Seeded Batch Crystallization Model. By studying the nature of the dynamic uncertainty plots of the process variables and their correlation to Ito processes, it has been observed that the uncertainties can be best modeled with a simple Ito process known as Brownian motion with drift.[19,27] It is defined as

$$dy = a(y, t)\,dt + b(y, t)\,dz \tag{25}$$

where dz is the increment of the Wiener process equal to $\varepsilon_t(\Delta t)^{1/2}$, and $a(y,t)$ and $b(y,t)$ are known functions. The random value ε_t has a unit normal distribution with zero mean and a standard deviation of 1. To estimate the values of the functions a and b, a generalized method presented by Diwekar[19] has been used (details are shown in Appendix B.1). In this paper, a simplification of the above equation is used to represent the time-dependent uncertainties in the concentration, seed, and nucleation moments:

$$dY_i = f(\overline{Y}_i, t)\Delta t + g_i\varepsilon_i\sqrt{\Delta t} \tag{26}$$

$$dy_1 = [-3\rho k_v G(t)(y_4 + y_8)]\Delta t + g_1\varepsilon_1\sqrt{\Delta t} \tag{27}$$

$$dy_2 = 0 \tag{28}$$

dx.doi.org/10.1021/ie300491v | Ind. Eng. Chem. Res. 2013, 52, 108−122

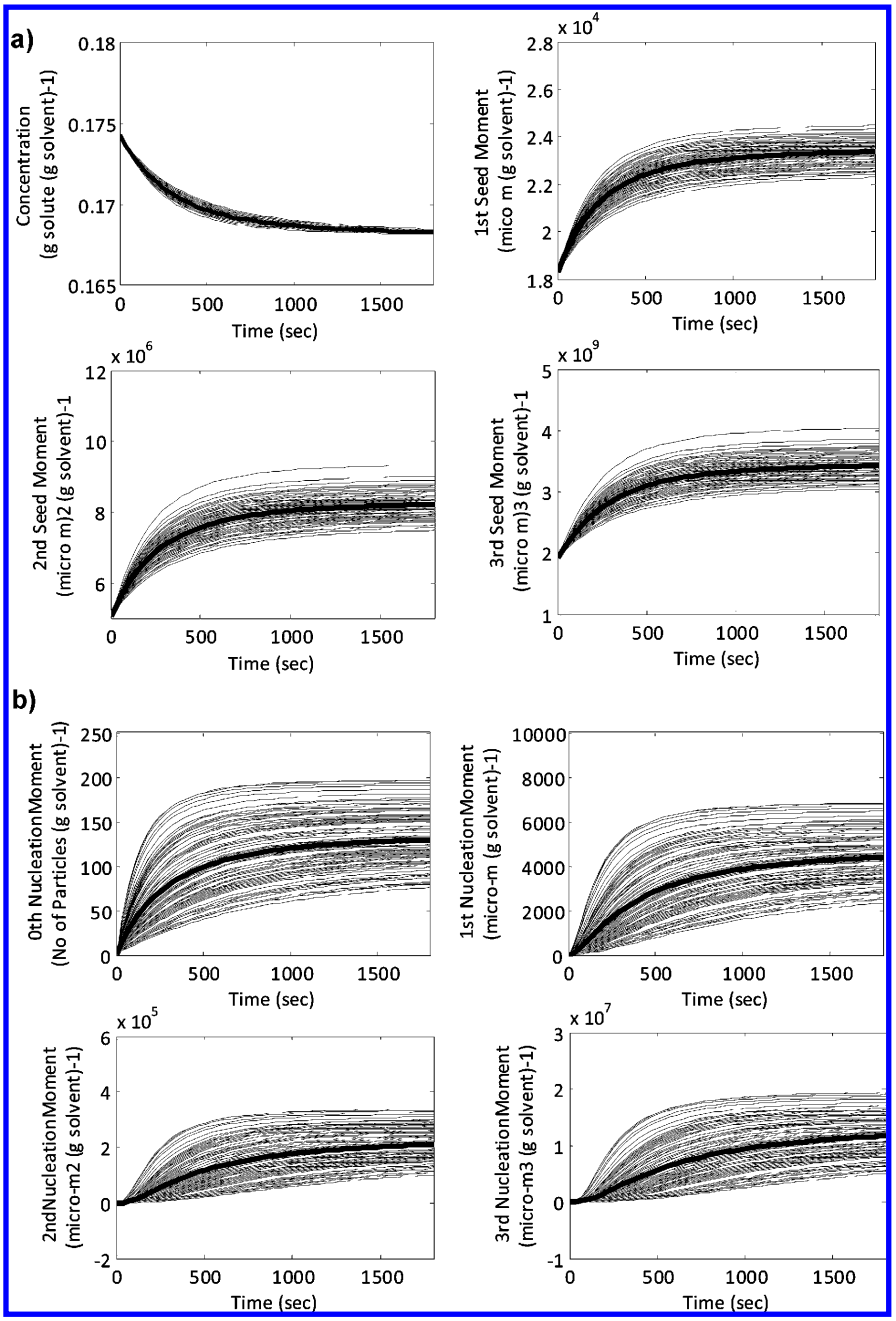

Figure 5. Dynamic uncertainties in (a) state variables C, μ_1^s, μ_2^s, μ_3^s and (b) state variables μ_0^n, μ_1^n, μ_2^n, μ_3^n.

$$dy_3 = (G(t)y_2)\Delta t + g_3\varepsilon_3\sqrt{\Delta t} \quad (29)$$

$$dy_4 = (2G(t)y_3)\Delta t + g_4\varepsilon_4\sqrt{\Delta t} \quad (30)$$

$$dy_5 = (3G(t)y_4)\Delta t + g_5\varepsilon_5\sqrt{\Delta t} \quad (31)$$

$$dy_6 = (B(t))\Delta t + g_6\varepsilon_6\sqrt{\Delta t} \quad (32)$$

$$dy_7 = (G(t)y_6)\Delta t + g_7\varepsilon_7\sqrt{\Delta t} \quad (33)$$

$$dy_8 = (2G(t)y_7(t))\Delta t + g_8\varepsilon_8\sqrt{\Delta t} \quad (34)$$

$$dy_9 = (3G(t)y_8(t))\Delta t + g_9\varepsilon_9\sqrt{\Delta t} \quad (35)$$

Here, the values of g_i are found using the method described in Appendix B.1. From the observations of the batch crystallization, static uncertainty parameters, and their effects within the state variables, we obtain the g-values shown in Table 4. Furthermore, the above equations are integrated using stochastic calculus,

Table 4. Coefficients in the Uncertainty Term of State Variables

parameter	value	parameter	value
g_1	2.659×10^{-5}	g_6	0.5486
g_2	0	g_7	25.91599
g_3	25.882	g_8	1382.3464
g_4	1.517×10^4	g_9	8.7453×10^4
g_5	6.57×10^6		

dx.doi.org/10.1021/ie300491v | Ind. Eng. Chem. Res. 2013, 52, 108−122

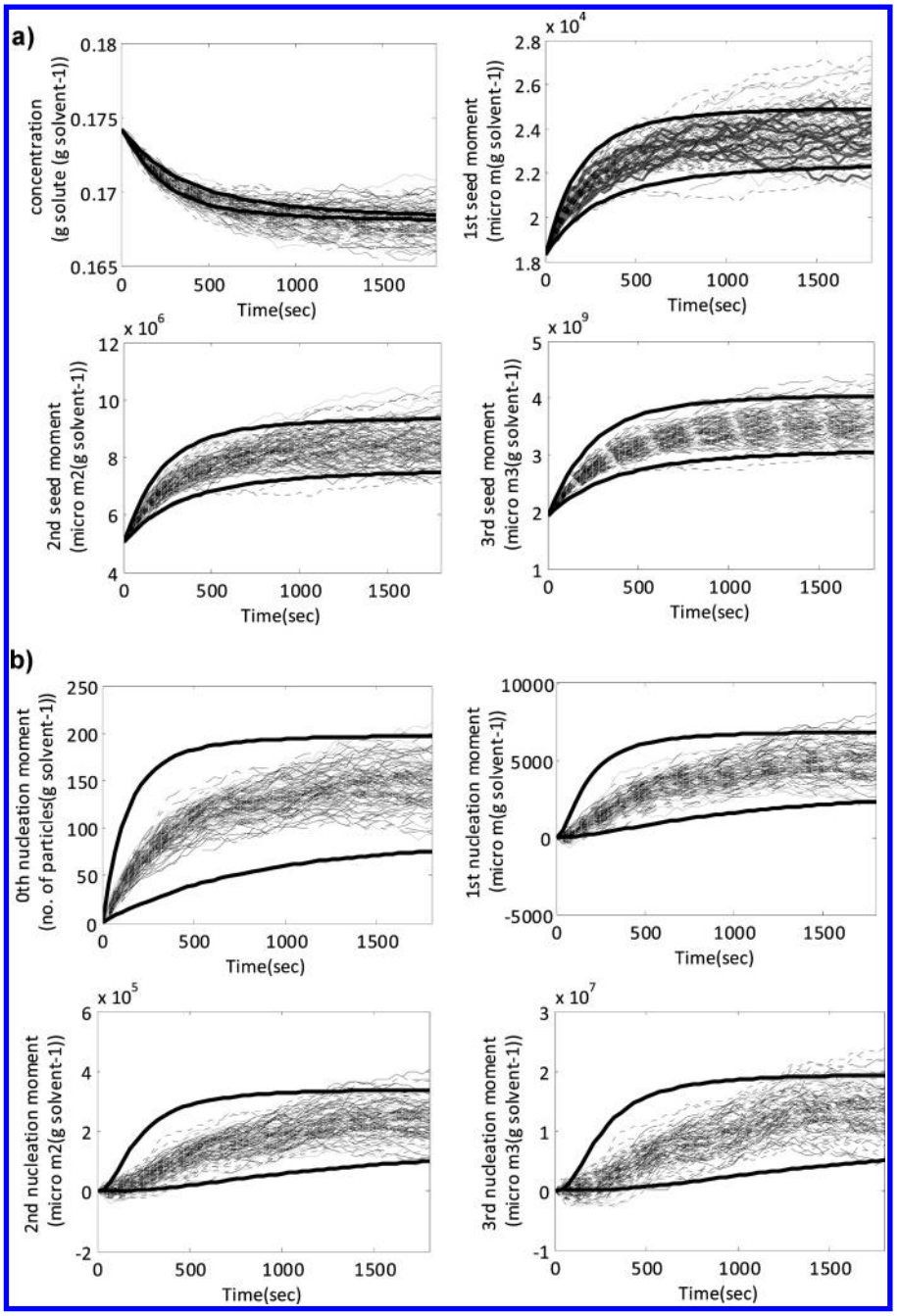

Figure 6. State variables modeled as Ito processes: (a) C, μ_1^s, μ_2^s, μ_3^s and (b) μ_0^n, μ_1^n, μ_2^n, μ_3^n.

which facilitates the integration of stochastic differential equations. We use a strong Taylor approximation—the Euler Maruyama scheme (as reported by Kloeden and Platen[28])—to integrate the stochastic differential equations numerically. It is the simplest strong Taylor approximation scheme, with an order of convergence of 0.5. The integration of the stochastic differential equations yield the results shown in Figures 6a and 6b. Thus, the representation as Ito processes can capture the dynamic uncertainties shown earlier in Figure 5.

5. OPTIMIZATION UNDER UNCERTAINTY

5.1. Stochastic Maximum Principle. We use the stochastic maximum principle, which is similar to the method illustrated in Ramirez and Diwekar.[23] The objective is to maximize the expected value of mass of seeded crystals and minimize the expected value of mass of fines, taken into account the uncertainties associated with the concentration and moments of batch crystallization, finding the best operating temperature profile for the process.

The objective function for the stochastic formulation can be written as eq 36a or eq 36b, where E is the expected value.

$$\max_T L = E\left[\int_t^0 \left\{\frac{d\mu_3^s}{dt} - \frac{d\mu_3^n}{dt}\right\} dt\right] \tag{36a}$$

$$\max_T L = E[\mu_3^s(t_f) - \mu_3^n(t_f)] \tag{36b}$$

subject to seeded batch crystallization, state variables modeled as Ito processes (eqs 26−35), initial conditions (see Table 2), and constraints for supersaturation condition maintenance

dx.doi.org/10.1021/ie300491v | Ind. Eng. Chem. Res. 2013, 52, 108−122

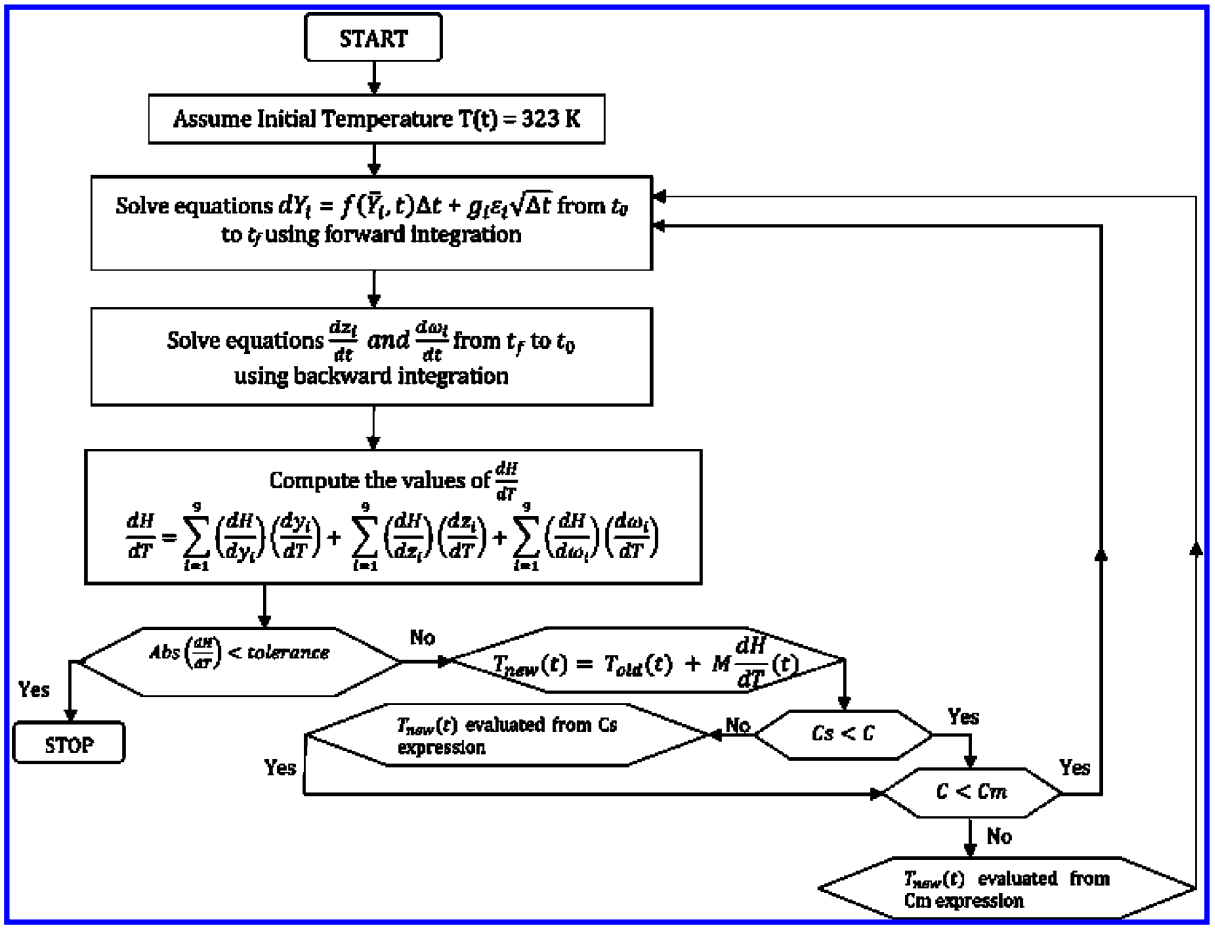

Figure 7. Flowchart for optimal temperature profile evaluation using stochastic maximum principle (active constraint strategy).

(see eq 16). The state equations generally can be represented as shown in eq 37:

$$dy_i = f(\bar{y}_i, t)\Delta t + g_i\varepsilon_i\sqrt{\Delta t} \tag{37}$$

where

$$y_i = [C \quad \mu_0^s \quad \mu_1^s \quad \mu_2^s \quad \mu_3^s \quad \mu_0^n \quad \mu_1^n \quad \mu_2^n \quad \mu_3^n]$$

The optimality condition[23] for the problem is given by eq 38.

$$0 = \max_T\left[k + \frac{1}{dt}E(dL)\right] \tag{38}$$

We use Ito's lemma for evaluating integrals for the stochastic differential equations. It is the stochastic counterpart of the chain rule in ordinary calculus. The terms are obtained by retaining the second-order Taylor series expansion term, which accounts for the change in the stochastic component of the process. Upon application of Ito's lemma to the optimality condition ($k = 0$), we get

$$0 = \frac{\partial L}{\partial t} + \sum_{i=1}^{9}\frac{\partial L}{\partial Y_i}F_i(Y_t, T_t) + \sum_{i=1}^{9}\frac{g_i^2}{2}\frac{\partial^2 L}{\partial Y_i^2} + \sum_{i\neq j}^{9} g_i^2 g_j^2\frac{\partial^2 L}{\partial Y_i \partial Y_j} \tag{39a}$$

$$0 = \frac{\partial L}{\partial t} + \mathrm{Max}\left[\frac{\partial L}{\partial Y_1}F_1 + \frac{\partial L}{\partial Y_2}F_2 + \frac{\partial L}{\partial Y_3}F_3 + \frac{\partial L}{\partial Y_4}F_4 + \frac{\partial L}{\partial Y_5}F_5 + \frac{\partial L}{\partial Y_6}F_6 + \frac{\partial L}{\partial Y_7}F_7 + \frac{\partial L}{\partial Y_8}F_8 + \frac{\partial L}{\partial Y_9}F_9 + \frac{g_{Y1}^2}{2}\frac{\partial^2 L}{\partial Y_1^2} + \frac{g_{Y2}^2}{2}\frac{\partial^2 L}{\partial Y_2^2} + \frac{g_{Y3}^2}{2}\frac{\partial^2 L}{\partial Y_3^2} + \frac{g_{Y4}^2}{2}\frac{\partial^2 L}{\partial Y_4^2} + \frac{g_{Y5}^2}{2}\frac{\partial^2 L}{\partial Y_5^2} + \frac{g_{Y6}^2}{2}\frac{\partial^2 L}{\partial Y_6^2} + \frac{g_{Y7}^2}{2}\frac{\partial^2 L}{\partial Y_7^2} + \frac{g_{Y8}^2}{2}\frac{\partial^2 L}{\partial Y_8^2} + \frac{g_{Y9}^2}{2}\frac{\partial^2 L}{\partial Y_9^2}\right] \tag{39b}$$

where

$$\frac{\partial L}{\partial Y_i} = z_i \quad \text{and} \quad \frac{\partial^2 L}{\partial Y_i^2} = \omega_i \tag{40}$$

Thus, eq 39b, in terms z_i and ω_i, is shown in eq 41:

$$0 = \frac{\partial L}{\partial t} + \mathrm{Max}\left[z_1F_1 + z_2F_2 + z_3F_3 + z_4F_4 + z_5F_5 + z_6F_6 + z_7F_7 + z_8F_8 + z_9F_9 + \omega_1\frac{g_{Y1}^2}{2} + \omega_2\frac{g_{Y2}^2}{2} + \omega_3\frac{g_{Y3}^2}{2} + \omega_4\frac{g_{Y4}^2}{2} + \omega_5\frac{g_{Y5}^2}{2} + \omega_6\frac{g_{Y6}^2}{2} + \omega_7\frac{g_{Y7}^2}{2} + \omega_8\frac{g_{Y8}^2}{2} + \omega_9\frac{g_{Y9}^2}{2}\right] \tag{41}$$

dx.doi.org/10.1021/ie300491v | Ind. Eng. Chem. Res. 2013, 52, 108−122

The stochastic Hamiltonian involves additional terms, compared to the deterministic system, and can be generalized as eq 42:

$$H = \sum_{i=1}^{9}\left(z_i F_i + \omega_i \frac{g_{Yi}^2}{2}\right) \tag{42}$$

$$H = z_1F_1 + z_2F_2 + z_3F_3 + z_4F_4 + z_5F_5 + z_6F_6 + z_7F_7 + z_8F_8 + z_9F_9 + \omega_1\frac{g_{Y1}^2}{2} + \omega_2\frac{g_{Y2}^2}{2} + \omega_3\frac{g_{Y3}^2}{2} + \omega_4\frac{g_{Y4}^2}{2} + \omega_5\frac{g_{Y5}^2}{2} + \omega_6\frac{g_{Y6}^2}{2} + \omega_7\frac{g_{Y7}^2}{2} + \omega_8\frac{g_{Y8}^2}{2} + \omega_9\frac{g_{Y9}^2}{2} \tag{43}$$

The adjoint equation formulas for the stochastic formulation are shown below in eqs 44 and 45. The final conditions for the adjoint variables are known and, again, we encounter a two-point boundary value problem to be solved.

$$\frac{dz_j}{dt} = \sum_{i=1}^{9}\left[-\frac{\partial F_i}{\partial Y_j}z_i - \frac{1}{2}\left(\frac{\partial g_i^2}{\partial Y_j}\right)\omega_i\right] \tag{44}$$

$$\frac{d\omega_j}{dt} = \sum_{i=1}^{9}\left[-2\omega_i\frac{\partial F_i}{\partial Y_j} - z_i\frac{\partial^2 F_i}{\partial Y_j^2} - \frac{1}{2}\left(\frac{\partial^2(g_i^2)}{\partial Y_j^2}\right)\omega_i\right] \tag{45}$$

Using methodology similar to that employed in deterministic control, we evaluate the optimal temperature profile. The difference lies in the equations for the state variables involving a stochastic term, along with the original differential function and two sets of adjoint variables, which are integrated in backward direction. The decision vector, which is the temperature at each time step, is obtained using the optimality condition for the Hamiltonian gradient to be less than the tolerance limit ($|dH/dT| < tolerance$) and also the active constraint for the concentration must be satisfied. The solution technique is presented in the flowchart shown in Figure 7. In this case, the derivative of the Hamiltonian includes its derivatives with respect to adjoint variables z_i and ω_i. The calculation method for the Hamiltonian derivative is shown in Appendix B.2.

To get a clear idea about the particle size, we try to recover the particle size distribution (PSD) in the form of probability density functions for seed and nucleated crystals separately. Since particle size uniformity is a characteristic of crystal purity, we use methods to recover the particle size distribution from the moment values.[29] We assume a known distribution for both the seed and nucleated crystals. Then, using the known moment values from the model, we evaluate the parameters for the distribution. In this case, we use the normal distribution (eq 46) to be the initially assumed distribution. Using eqs 47−49, we evaluate the mean values and the standard deviations.

$$f(x) = \frac{1}{\sigma\sqrt{2\pi}}\exp\left\{-\frac{(x-\bar{x})^2}{2\sigma^2}\right\} \tag{46}$$

$$\bar{x} = \frac{\mu_1}{\mu_0} \tag{47}$$

$$c_v = \sqrt{\frac{\mu_0\mu_2}{\mu_1^2} - 1} \tag{48}$$

$$\sigma = \bar{x}c_v \tag{49}$$

5.2. Results and Discussions. The derivative of Hamiltonian profiles at different iterations are shown in Figure 8. It can be seen that the $|dH/dT|$ value decreases with every iteration. The temperature profiles can be observed in Figure 9 for all iterations, and the final iteration is shown as a bold line. In comparison with the deterministic profile, the temperature decrease is much steeper, since the stochasticity (ω_i) has been taken into account within the Hamiltonian and its gradient.

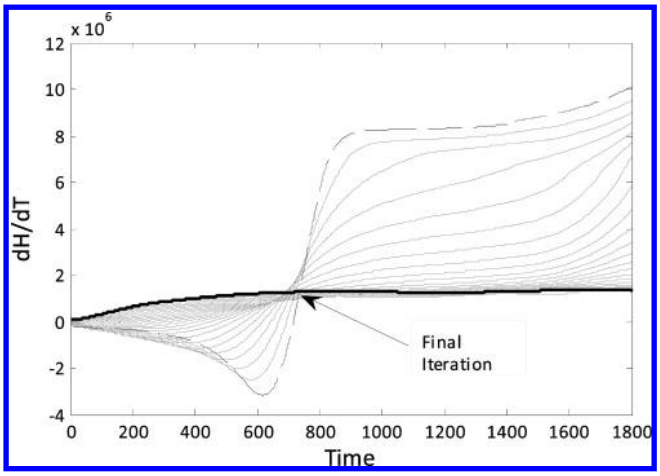

Figure 8. Profiles of Hamiltonian gradients for all iterations.

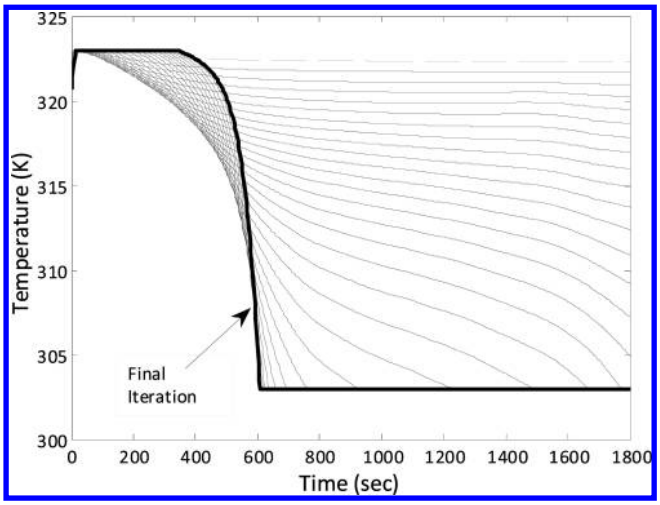

Figure 9. Profiles of temperature for all iterations.

The objective functions are evaluated using the stochastic optimal temperature trajectory for all 100 samples evaluated earlier from the uncertain kinetic parameter data (Table 3). Thus, we get 100 profiles for our objective function, whose expected value is evaluated using the method of averages, shown as the bold line in Figure 10. This average value represents the most likely objective function value to be attained when the batch crystallizer is operated under the stochastic optimal temperature profile.

Figure 11 summarizes the optimal temperature profiles evaluated using the deterministic method and the stochastic method. The results for the linear cooling profile, which is most commonly used, are also compared against the optimal

dx.doi.org/10.1021/ie300491v | Ind. Eng. Chem. Res. 2013, 52, 108−122

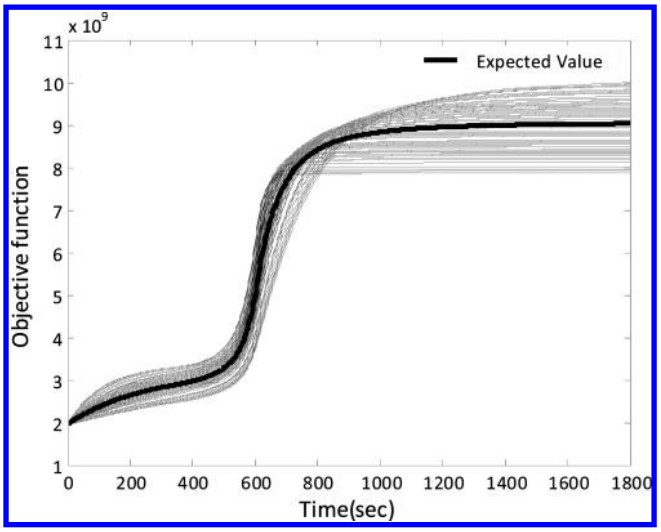

Figure 10. Objective functions for the stochastic case with the expected value.

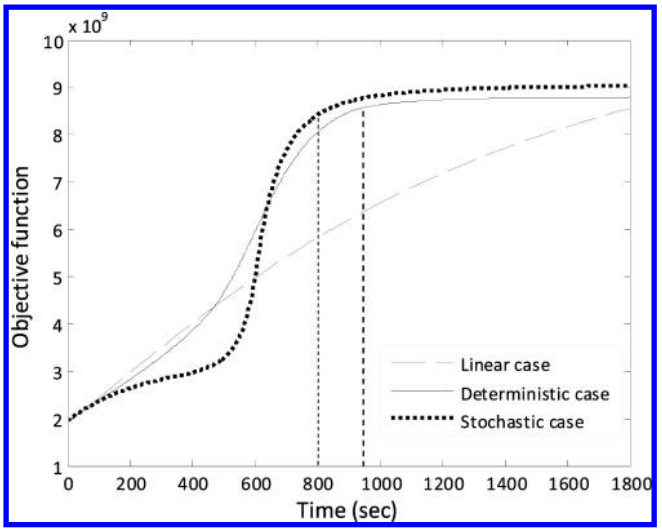

Figure 12. Comparison of the objective function $\exp[\mu_3^s(t_f) - \mu_3^n(t_f)]$ (linear, deterministic, and stochastic cases).

trajectories. The temperature profile for the stochastic case shows an initial lag in the temperature decrease, then a much steeper decrease is observed in its value, compared to the deterministic case. This may be due to the derivative values of the Hamiltonian evaluated from the stochastic calculus, which may allow the temperature to reach a better optimal value.

Figure 12 shows the comparison of the objective function values for the linear cooling profile, deterministic optimal temperature trajectory, and stochastic optimal temperature profile under the presence of uncertainty. The objective function for all three cases is the expected value of the 100 evaluated functions for each case, respectively. It also shows that the deterministic and stochastic profiles reach the optimum in much lesser time, compared to the linear case. Thus, using the optimal trajectory ensures better crystal size distribution by ensuring the values of the representative moments to be optimum. The objective, which is the difference between the third seed and nucleation moment, shows that the optimal profiles favor growth of the seeded crystals and their growth is maximum under the stochastic optimal temperature. We can also observe the fact that the time needed to reach an acceptable range of the objective function generally desired is much lesser for the deterministic (950 s) and stochastic (800 s) cases, compared to linear cooling (1800 s).

Table 5 shows a summary of the results for the three cases considered. The objective function value is the difference

Table 5. Results of a Comparison between the Linear, Deterministic, and Stochastic Cases

case	objective function	% increment in stochastic case	time to reach the similar objective function value (s)
linear	8.53×10^9	5.88	1800
deterministic	8.79×10^9	2.73	950
stochastic	9.03×10^9	N.A.	800

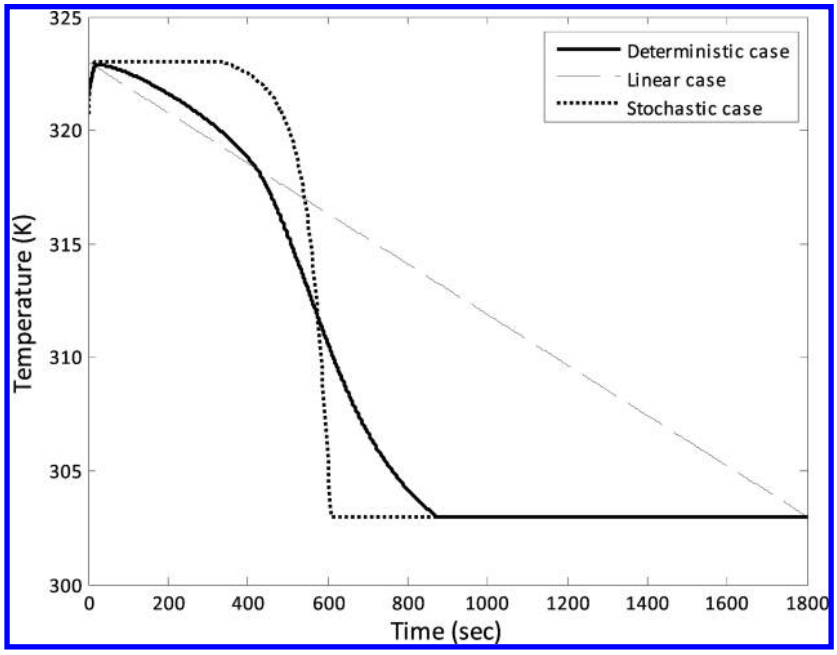

Figure 11. Comparison of temperature profiles (linear, deterministic, and stochastic cases).

dx.doi.org/10.1021/ie300491v | Ind. Eng. Chem. Res. 2013, 52, 108−122

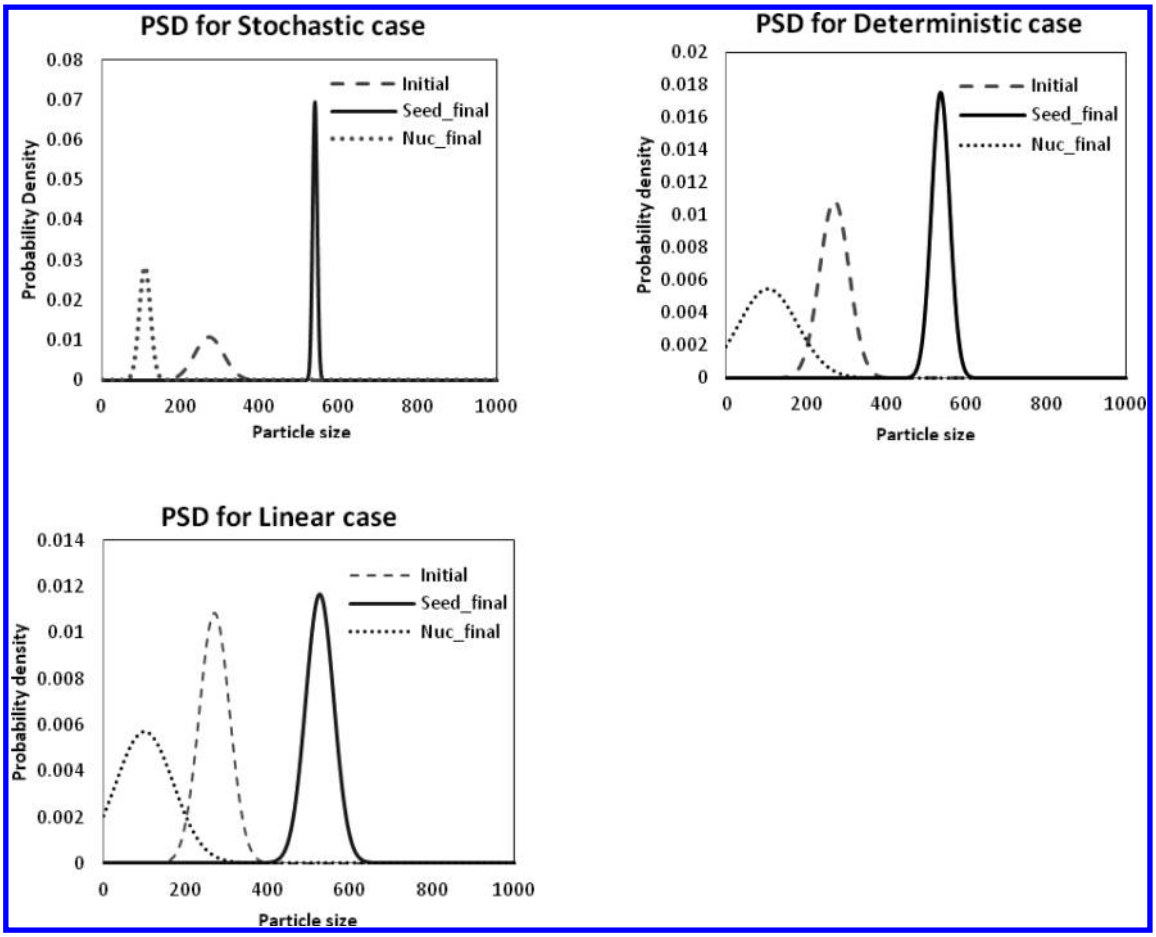

Figure 13. Comparison of size distribution for the linear, deterministic, and stochastic cases.

between the third seed moment and the third nucleation moment at the final batch time. The stochastic case shows better results when compared to both linear case (5.88%) and deterministic case (2.73%) in the presence of uncertainty.

Figure 13 compares the PSD for the three cases (linear, deterministic, and stochastic). It should be noted that the distributions are in the form of probability density functions and, hence, do not give an exact idea about the number of crystals; however, they provide a tool for comparing the crystal size for the three cases. It can be seen that the objective to have maximum growth of seeded crystals with maximum size uniformity is very well satisfied for the stochastic case. The deterministic case has better results over the linear case; however, in the presence of uncertainty, the stochastic case proves to be better than both cases.

6. CONCLUSIONS

In the present work, the kinetic parameter uncertainty present in batch crystallization models is considered for analysis, and its effect on the overall process performance is evaluated in terms of the control variable: temperature. The static uncertainty in the kinetics results in dynamic uncertainties within the state variables. These uncertainties could be modeled as Ito processes, since they followed certain properties and had a behavioral pattern. The most important aspect was to solve the stochastic optimal control problem involving Ito processes and application of stochastic calculus, Ito's lemma, and stochastic maximum principle. Application of optimal temperature trajectories against the simple linear cooling profile provided much better crystal size distributions (measured in terms of moments). The significant difference in the batch time needed to reach the optima and the difference in the particle size distributions for the three cases help in realizing the importance of uncertainty consideration during the modeling and control of industrial crystallization.

APPENDIX A.1: DETAILS OF THE DETERMINISTIC MODEL

The nine state equations for the seeded batch crystallization model are as stated below, along with the deterministic Hamiltonian. The adjoint equations are given in eqs A.11−A.19.

$$\frac{dy_1}{dt} = -3\rho k_v G(t)(y_4 + y_8) \tag{A.1}$$

$$\frac{dy_2}{dt} = 0 \tag{A.2}$$

$$\frac{dy_3}{dt} = G(t)y_2 \tag{A.3}$$

$$\frac{dy_4}{dt} = 2G(t)y_3 \tag{A.4}$$

$$\frac{dy_5}{dt} = 3G(t)y_4 \tag{A.5}$$

dx.doi.org/10.1021/ie300491v | Ind. Eng. Chem. Res. 2013, 52, 108−122

$$\frac{dy_6}{dt} = B(t) \tag{A.6}$$

$$\frac{dy_7}{dt} = G(t)y_6 \tag{A.7}$$

$$\frac{dy_8}{dt} = 2G(t)y_7 \tag{A.8}$$

$$\frac{dy_9}{dt} = 3G(t)y_8 \tag{A.9}$$

Hamiltonian for the system:

$$H = z_1\left[-3\rho k_v G(t)(y_4 + y_8)\right] + z_2 0 + z_3 G(t)y_2 + z_4 2G(t)y_3 + z_5 3G(t)y_4 + z_6 B(t) + z_7 G(t)y_6 + z_8 2G(t)y_7 + z_9 3G(t)y_8 \tag{A.10}$$

Adjoint equations corresponding to the state equations:

$$\frac{dz_1}{dt} = -z_1\left\{-3\rho k_v(y_4 + y_8)\left[\frac{\partial G(t)}{\partial y_1}\right]\right\} - \left\{(z_3 y_2 + 2z_4 y_3 + 3z_5 y_4 + z_7 y_6 + 2z_8 y_7 + 3z_9 y_8)\left[\frac{\partial G(t)}{\partial y_1}\right]\right\} - z_6\left[\frac{\partial B(t)}{\partial y_1}\right] \tag{A.11}$$

$$\frac{dz_2}{dt} = -z_3 G(t) \tag{A.12}$$

$$\frac{dz_3}{dt} = -2z_4 G(t) \tag{A.13}$$

$$\frac{dz_4}{dt} = 3z_1\rho k_v G(t) - 3z_5 G(t) \tag{A.14}$$

$$\frac{dz_5}{dt} = -z_6 k_b \exp\left(\frac{-E_b}{RT}\right)S^b \tag{A.15}$$

$$\frac{dz_6}{dt} = -z_7 G(t) \tag{A.16}$$

$$\frac{dz_7}{dt} = -2z_8 G(t) \tag{A.17}$$

$$\frac{dz_8}{dt} = 3z_1\rho k_v G(t) - 3z_9 G(t) \tag{A.18}$$

$$\frac{dz_9}{dt} = -z_6 k_b \exp\left(\frac{-E_b}{RT}\right)S^b \tag{A.19}$$

where

$$\frac{\partial G}{\partial y_1} = k_g g \exp\left(\frac{-E_g}{RT}\right)S^{(g-1)}\left(\frac{1}{Cs}\right)$$

$$\frac{\partial B}{\partial y_1} = k_b b \exp\left(\frac{-E_b}{RT}\right)S^{(b-1)}\left(\frac{1}{Cs}\right)(y_4 + y_8)$$

APPENDIX A.2: CALCULATION OF THE HAMILTONIAN DERIVATIVE IN THE DETERMINISTIC CASE

Since the maximum principle involves the maximization of Hamiltonian over the control variable, the optimality condition is $|dH/dT|$ < tolerance. The derivative evaluation of the Hamiltonian, with respect to the control variable (temperature), is shown later. Here, the Hamiltonian is a function of several variables such as t, y, z, T; hence, its derivative can be expressed as a sum of partial derivatives, with respect to each of these variables. To illustrate this, let us consider a function $P = f(x,y)$ of several variables t, x, y. The complete derivative, with respect to one variable (t), is given by eq A.20:

$$\frac{dP}{dt} = \frac{\partial P}{\partial x}\left(\frac{dx}{dt}\right) + \frac{\partial P}{\partial y}\left(\frac{dy}{dt}\right) \tag{A.20}$$

Upon application of this total derivative method to the Hamiltonian shown in eq A.10, we get

$$\frac{dH}{dT} = \sum_{i=1}^{9}\left(\frac{dH}{dy_i}\right)\theta_i + \sum_{i=1}^{9}\left(\frac{dH}{dz_i}\right)\phi_i \tag{A.21}$$

where θ_i and ϕ_i are represented by eqs A.22 and A.23, respectively:

$$\theta_i = \left(\frac{dy_i}{dT}\right) \tag{A.22}$$

$$\phi_i = \left(\frac{dz_i}{dT}\right) \tag{A.23}$$

The following differential equations are used to evaluate θ_i and ϕ_i:

$$\frac{d\left(\frac{dy_i}{dt}\right)}{dT} = \frac{d\left(\frac{dy_i}{dT}\right)}{dt} = \frac{d\theta_i}{dt} \tag{A.24}$$

$$\frac{d\left(\frac{dz_i}{dt}\right)}{dT} = \frac{d\left(\frac{dz_i}{dT}\right)}{dt} = \frac{d\phi_i}{dt} \tag{A.25}$$

Thus, the general form of these two equations, in terms of the associated variables, can be written as

$$\frac{d\theta_i}{dt} = f(y_i, \theta_i, T) \tag{A.26}$$

$$\frac{d\phi_i}{dt} = f(y_i, \theta_i, z_i, \phi_i, T) \tag{A.27}$$

For example, if we consider the equation of the third moment of seed (i.e., eq A.5),

$$\frac{d\theta_5}{dt} = 3y_4\frac{dG(t)}{dT} + 3G(t)\theta_4 \tag{A.28}$$

$$\frac{d\phi_5}{dt} = -k_b \exp\left(\frac{-E_b}{RT}\right)\left\{\left[z_6 S^b\left(\frac{E_b}{RT^2}\right)\right] + \left[z_6 b S^{(b-1)}\frac{dS}{dT}\right] + [\phi_6 S^b]\right\} \tag{A.29}$$

Equation A.26 is integrated in the forward direction, using a numerical method, with the initial conditions of

dx.doi.org/10.1021/ie300491v | Ind. Eng. Chem. Res. 2013, 52, 108−122

$\theta_i(t_0) = [0\,0\,0\,0\,0\,0\,0\,0\,0\,0]$, while eq A.27 is integrated in the backward direction, with the final boundary conditions of $\oint(t_f) = [0\,0\,0\,0\,0\,0\,0\,0\,0\,0]$.

APPENDIX A.3: THE TEMPERATURE EVALUATION FROM THE CONSTRAINT CONDITION

After the updated temperature obtained from the update expression A.30, we check for the concentration constraint to be active. We have the concentration value at that time point in $y_1(t)$. We compare $y_1(t)$ values with C_s and C_m. The active constraint is given by the following condition:

$$C_s \le C \le C_m$$

$$T(t)_{\text{new}} = T(t)_{\text{new}} + M\left.\frac{dH}{dT}\right|_t \tag{A.30}$$

If $C_s \le C$ or $y_1(t)$ is not satisfied, then we impose the concentration value at that time to be C_s and, hence, evaluate the temperature from the expression for C_s (note that the expression is for temperature in units of °C). We get a quadratic expression in terms of temperature (eq A.31), which yields two values for temperature, one of which is feasible and is accepted as the optimal temperature at that time point.

$$y_1(t) = 6.29 \times 10^{-2} + 2.46 \times 10^{-3}T - 7.14 \times 10^{-6}T^2 \tag{A.31}$$

APPENDIX B.1: EVALUATION METHOD FOR PARAMETERS IN THE EQUATION FOR BROWNIAN MOTION WITH DRIFT

Consider an Ito process or stochastic process $x(t)$, in which the increment dx is represented as eq B.1:

$$dx = a(x, t)\,dt + b(x, t)\,dz \tag{B.1}$$

The general expression for Brownian motion with drift is represented as eq B.2:

$$dx = \alpha\,dt + \sigma\,dz \tag{B.2}$$

where α is the drift parameter and σ is the variance parameter. The discretized version of eq B.1 can be written as eq B.3:

$$x_t = x_{t-1} + \alpha\Delta t + \sigma\epsilon_t\sqrt{\Delta t} \tag{B.3}$$

ϵ_t is normally distributed with a mean value of 0 and a standard deviation of 1.0. Hence, over any time interval Δt, the change in x is normally distributed and has an expected value of variance. To evaluate α, the average value of the difference in x ($E[x_t - x_{t-1}]$) is computed and divided by the time interval Δt. For σ, the variance of the differences in x is found, divided by the time interval Δt, and then the square root of this value is taken. In this paper, the change in the function (i.e., the drift parameter) is the right-hand side (RHS) of the deterministic differential equations, but the value of the stochastic component g is evaluated as the method suggested for σ evaluation.

APPENDIX B.2: CALCULATION OF THE HAMILTONIAN DERIVATIVE IN THE STOCHASTIC CASE

The methodology is the same as shown in Appendix A.2, except that we have one more adjoint variable (ω). Hence, we have an additional variable (ψ) in the Hamiltonian gradient evaluation. Upon application of this total derivative method to the stochastic Hamiltonian, we get

$$\frac{dH}{dT} = \sum_{i=1}^{9}\left(\frac{dH}{dy_i}\right)\theta_i + \sum_{i=1}^{9}\left(\frac{dH}{dz_i}\right)\oint_i + \sum_{i=1}^{9}\left(\frac{dH}{d\omega_i}\right)\psi_i \tag{B.4}$$

where θ_i, $\oint_i$, and ψ_i are represented by eqs B.2, B.3, and B.4:

$$\theta_i = \left(\frac{dy_i}{dT}\right) \tag{B.5}$$

$$\oint_i = \left(\frac{dz_i}{dT}\right) \tag{B.6}$$

$$\psi_i = \left(\frac{d\omega_i}{dT}\right) \tag{B.7}$$

The following differential equations are used to evaluate θ_i and $\oint_i$:

$$\frac{d\left(\frac{dy_i}{dt}\right)}{dT} = \frac{d\left(\frac{dy_i}{dT}\right)}{dt} = \frac{d\theta_i}{dt} \tag{B.8}$$

$$\frac{d\left(\frac{dz_i}{dt}\right)}{dT} = \frac{d\left(\frac{dz_i}{dT}\right)}{dt} = \frac{d\oint_i}{dt} \tag{B.9}$$

$$\frac{d\left(\frac{d\omega_i}{dt}\right)}{dT} = \frac{d\left(\frac{d\omega_i}{dT}\right)}{dt} = \frac{d\psi_i}{dt} \tag{B.10}$$

Thus, the general form of these three equations, in terms of the associated variables, can be written as

$$\frac{d\theta_i}{dt} = f(y_i, \theta_i, T) \tag{B.11}$$

$$\frac{d\oint_i}{dt} = f(y_i, \theta_i, z_i, \oint_i, T) \tag{B.12}$$

$$\frac{d\oint_i}{dt} = f(y_i, \theta_i, z_i, \oint_i, \omega_i, \psi_i, T) \tag{B.13}$$

Equation B.11 is integrated in the forward direction, using a numerical method, with the initial conditions of $\theta_i(t_0) = [0\,0\,0\,0\,0\,0\,0\,0\,0\,0]$, while eqs B.12 and B.13 are integrated in the backward direction, with the final boundary conditions of $\oint_i(t_f) = [0\,0\,0\,0\,0\,0\,0\,0\,0\,0]$ and $\psi_i(t_f) = [0\,0\,0\,0\,0\,0\,0\,0\,0\,0]$.

AUTHOR INFORMATION

Corresponding Author

*E-mail: urmila@vri-custom.org.

Notes

The authors declare no competing financial interest.

NOMENCLATURE

$n(r,t)$ = number of crystals of radius r at time t
$G(r,t)$ = growth rate of crystals of radius r at time t
B = nucleation rate
C = concentration of solute in the solution
C_s = saturation concentration of solute in solution
C_m = metastable concentration of solute in the solution
T = temperature
μ_i = ith moment of crystallization
k_b = nucleation kinetic constant
k_g = growth kinetic constant

dx.doi.org/10.1021/ie300491v | Ind. Eng. Chem. Res. 2013, 52, 108−122

E_b = activation energy for nucleation
E_g = activation energy for growth
b = nucleation exponent
g = growth exponent
μ_i^n = ith nucleation moment
μ_i^s = ith seed moment
ρ = density of crystals
k_v = shape factor of crystals
H = Hamiltonian
dH/dT = derivative of Hamiltonian, with respect to temperature
R = universal gas constant
t = time (s)
y_i = state variable
z_i, w_i = adjoint variables
θ_i, ϕ_i, ψ_i = auxiliary variables for dH/dT evaluation

REFERENCES

(1) Costa, C. B. B.; da Costa, A. C.; Filho, R. M. Mathematical modeling and optimal control strategy development for an adipic acid crystallization process. *Chem. Eng. Process.* **2005**, *44*, 737−753.
(2) Priscilla, J. Hill; Korovessi, E. L; Linninger, A. A. *Batch Processes: Batch Crystallization*; CRC Press/Taylor & Francis: New York, 2006.
(3) Randolph, A. D.; Larson, M. A. *Theory of Particulate Processes: Analysis and Techniques of Continuous Crystallization*, 2nd ed.; Academic Press: San Diego, CA, 1988.
(4) Mullin, J. W. *Crystallization*, 3rd ed.; Butterworth−Heinemann: London, 1993.
(5) Ward, J. D.; Mellichamp, D. A.; Doherty, M. F. Choosing an operating policy for seeded batch crystallization. *AIChE J.* **2006**, *52*, 2046−2054.
(6) Mulin, J. W.; Nyvlt, J. Programmed cooling of batch crystallizers. *Chem. Eng. Sci.* **1971**, *26*, 369−377.
(7) Jones, A. G. Optimal operation of a batch cooling crystallizer. *Chem. Eng. Sci.* **1974**, *29*, 1075−1087.
(8) Rawlings, J. B.; Witkowski, W. R.; Eaton, J. W. Modeling and control of crystallizers. *Powder Technol.* **1992**, *69*, 3−9.
(9) Miller, S. M.; Rawlings, J. B. Model identification and control strategies for batch cooling crystallizers. *AIChE J.* **1994**, *40*, 1312−1327.
(10) Hu, Q.; Rohani, S.; Jutan, A. Modelling and optimization of seeded batch crystallizers. *Comput. Chem. Eng.* **2005**, *29*, 911−918.
(11) Shi, D.; El-Farra, N.; Li, M.; Mhaskar, P.; Christofides, P. D. Predictive control of particle size distribution in particulate processes. *Chem. Eng. Sci.* **2006**, *61*, 268−28.
(12) Paengjuntuek, W.; Arpornwichanop, A.; Kittisupakorn, P. Product quality improvement of batch crystallizers by a batch to batch optimization and non-linear control approach. *Chem. Eng. J.* **2008**, *139*, 344−350.
(13) Corriou, J. P.; Rohani, S. A new look at optimal control of a batch crystallizer. *AIChE J.* **2008**, *54*, 3188−3206.
(14) Chiu, T. Y.; Christofides, D. Robust control of particulate processes using uncertain population balances. *AIChE J.* **2000**, *46*, 266−280.
(15) Grosso, M.; Cogoni, G.; Baratti, R.; Romagnoli, J. A. Stochastic Approach for the prediction of PSD in crystallization processes: Formulation and comparative assessment of different stochastic models. *Ind. Eng. Chem. Res.* **2011**, *50*, 2133−2143.
(16) Laloue, N.; Couenne, F.; Gorrec, Y. L.; Kohl, M.; Tanguy, D.; Tayakout-Fayolle, M. Dynamic modelling of a batch crystallization process: A stochastic approach for agglomeration and attrition process. *Chem. Eng. Sci.* **2007**, *62*, 6604−6614.
(17) Ma, D. L.; Chung, S. H.; Braatz, R. D. Worst-case performance analysis of optimal batch control trajectories. *AIChE J.* **1999**, *45*, 1469−1476.
(18) Ma, D. L.; Braatz, R. D. Worst-case analysis of finite-time control policies. *IEEE Trans. Control Syst. Technol.* **2001**, *9*, 766−774.
(19) Diwekar, U. *Introduction to Applied Optimization*, 2nd ed.; Springer: New York, 2008.
(20) Kumar, S; Ramakrishna, D. On the solution of population balance equations by discretization−III. Nucleation, growth and aggregation of particles. *Chem. Eng. Sci.* **1997**, *52*, 4659−4679.
(21) Hu, Q; Rohani, S; Jutan, A. New numerical method for solving the dynamic population balance equations. *AIChE J.* **2005**, *51*, 3000−3006.
(22) Benavides, P. T.; Diwekar, U. Optimal control of biodiesel production in a batch reactor. Part I: Deterministic control. *Fuel* **2011**, DOI: 10.1016/j.fuel.2011.08.035.
(23) Rico-Ramirez, V.; Diwekar, U. M. Stochastic maximum principle for optimal control under uncertainty. *Comput. Chem. Eng.* **2004**, *28*, 2845−2849.
(24) Benavides, P. T.; Diwekar, U. Optimal control of biodiesel production in a batch reactor. Part II: Stochastic control. *Fuel* **2012**, *94*, 218−226.
(25) Ulas, S.; Diwekar, U. M. Thermodynamic uncertainties in batch processing and optimal control. *Comput. Chem. Eng.* **2004**, *28*, 2245−2258.
(26) Ulas, S.; Diwekar, U. M.; Stadtherr, M. A. Uncertainties in parameter estimation and optimal control in batch distillation. *Comput. Chem. Eng.* **2005**, *29*, 1805−1814.
(27) Wong, E.; Zakai, M. On the relation between ordinary and stochastic differential equations. *Int. J. Eng. Sci.* **1965**, *3*, 213−229.
(28) Kloeden, P. E.; Platen, E. *Numerical Solution of Stochastic Differential Equations*, 3rd ed.; Springer: New York, 1999.
(29) John, V.; Angelov, I.; Öncül, A. A.; Thévenin, D. Techniques for the reconstruction of a distribution from a finite number of its moments. *Chem. Eng. Sci.* **2007**, *62*, 2890−2904.